A general solution to the identification of moving vehicle forces on a bridge

A. González [1,*], C. Rowley[1] and E. J. OBrien[1]

[1]*UCD School of Architecture, Landscape and Civil Engineering, University College Dublin, Earlsfort Terrace, Dublin 2, Ireland*

[*]Corresponding author: Dr. Arturo Gonzalez, UCD School of Architecture, Landscape and Civil Engineering, UCD, Belfield, Dublin 4, Ireland.

SUMMARY

Bridge Weigh-In-Motion systems measure bridge strain caused by the passing of a truck to estimate static axle weights. For this calculation, they commonly use a static algorithm that takes the bridge influence line as reference. Such a technique relies on adequate filtering to remove bridge dynamics and noise. However, filtering can lead to the loss of a significant component of the underlying signal in bridges where the vibration does not have time to complete sufficient number of cycles, and in cases of closely spaced axles traveling at high vehicle speeds. In order to overcome these limitations and also to provide additional information on the dynamics of the applied forces, this paper presents an algorithm based on first order Tikhonov regularization and dynamic programming. First, strain measurements are simulated using an elaborate 3-D vehicle and orthotropic bridge interaction system. Then, strain is contaminated with noise and input into the moving force identification algorithm. The procedure to

implement the algorithm and to derive the applied forces from the simulated strain record is described. Vehicle axle forces are shown to be accurately predicted for smooth and rough road profiles and a range of speeds.

KEYWORDS: bridge dynamics; vehicle forces; noise; strain; inverse dynamics; weigh-in-motion

1. INTRODUCTION

A Bridge Weigh In Motion (B-WIM) system is based on the measurement of the deformation of a bridge and the use of the measurements to estimate the attributes of passing traffic loads. Considerable progress has been made in data acquisition hardware and software for B-WIM systems. This advance in data acquisition technology has allowed the measurement of voltage from axle detectors and a lot of strain sensors under the bridge soffit with good resolution and high scanning rates. Additionally, software has been developed to process this voltage information into vehicle classification and weights on a continuous basis [1].

Commercial B-WIM systems are commonly based on Moses' static algorithm [2], which assumes that a moving load will cause a bridge to bend in proportion to the product of the load magnitude and a reference curve representative of the bridge behavior, the influence line. The measured strain is the result of all axle forces that are on the bridge. On the one hand, this record can make it difficult to distinguish the contribution of each axle at each instant. On the other hand, a long continuous record of the whole truck weight is available. Hence, B-WIM systems will generally tend to be

more accurate for calculating gross weights than axle weights. Inaccurate assumed characteristics for influence lines, bridge and vehicle dynamics and the presence of noise have been shown to be significant sources of error for the traditional static B-WIM algorithm [3,4]. An accurate separation of dynamic and static components using filtering techniques is difficult to establish even at relatively high frequencies. The frequencies at which statics and dynamics are mixed together depend on a large number of parameters such as the vehicle speed, axle configuration, bridge length, stiffness and natural frequency, etc. This paper proposes a new B-WIM algorithm that increases the accuracy of B-WIM systems using moving force identification (MFI) theory to reduce the dynamic uncertainty associated to the bridge measurements.

There has been a significant amount of research in the field of MFI in recent years. Many of the current methods of MFI can be loosely divided into two categories, those that use the finite element method [5-8] and those that employ an exact solution method coupled with some form of system identification technique [9-13]. The solutions to the MFI problem using an exact solution method are generally subject to large fluctuations in the predicted force at the start and end of the time history due to the ill-conditioning of the least squares formulation of the problem. The method of Tikhonov regularisation [14] is employed to provide a bound to the error and smoother solutions to the MFI problem [15-20].

Much of the attention of MFI theory has focused on the use of one-dimensional beam models to represent the dynamics of the bridge. In many cases this is not an accurate representation of the bridge characteristics as torsional and lateral modes of vibration

can have a significant effect on the overall behaviour of the structure. Nevertheless, there has been some research to extend the theory to two and three dimensions. So, Zhu et al modelled the bridge deck as an orthotropic plate subject to moving forces [21,22,23]. The moving forces were idealised as a group of two moving forces representing two individual axles or a group of four moving forces representing each wheel load. The equilibrium equation of motion was reduced to decoupled equation in modal coordinates using the principle of modal superposition, and solved for in the time domain using the convolution integral. The problem was then formulated as a least squares with Tikhonov regularisation using strains or accelerations as the measured input [21,22]. Alternatively, displacements can be used as the measured input and related to the modal displacements via a least formulation, where the modal accelerations and velocities can be calculated using some form of numerical differentiation or a dynamic programming filter [23]. The problem of predicting the moving forces is again formulated as a least squares with Tikhonov regularisation [24].

The method of dynamic programming with Tikhonov regularization to solve inverse structural dynamics problems was first formulated by Trujillo [25]. This method has been previously applied to the MFI problem on a simply supported bridge model using the zeroth order regularization [26]. In this paper, the MFI problem is solved using first order Tikhonov regularization on a two-dimensional orthotropic plate bridge model. The finite element (FE) method is used to discretize the bridge into an equivalent dynamic model. Truck wheels are idealized as individual moving forces. The problem is then formulated as a least squares minimization of the difference between measured and theoretical strain, and a regularization technique is employed to reduce the errors of the

ill-conditioned system. The method of dynamic programming is used to solve the recursive least squares formulation. An eigenvalue reduction technique is also applied to reduce the dimension of the system in the dynamic programming routine. The algorithm is tested using the simulated strain from an independently built 3-D vehicle-bridge interaction (VBI) MSc/NASTRAN FE model that is further contaminated with 2% Gaussian noise.

2. SIMULATION OF THE STRAINS CAUSED BY THE PASSAGE OF A TRUCK OVER A BRIDGE

This section presents the simulation technique employed to obtain the bridge strain data that will be used for testing the MFI B-WIM algorithm. Truck and bridge have been modeled with the general-purpose FE package MSc/NASTRAN for Windows [27]. The authors use an approach based on a Lagrange technique that allows for the representation of the compatibility condition at the bridge/vehicle interface through a set of auxiliary functions [28,29]. Accordingly, software has been developed to generate an entry into the assembled stiffness matrix of the vehicle-bridge system provided by MSc/NASTRAN [4]. This entry allows for the definition of the forces acting on the bridge due to the moving wheels. A compatibility condition between the vertical displacement of the wheel, the road profile irregularities and the bridge at the contact point has also been established.

The bridge deck is idealized as a 20 m long single span orthotropic slab, made of plate elements with uniform thickness and density properties. The deck has a voided cross-

section of 0.8 m depth with voids of approximatly .6 m at 1.2 m spacing, 9 m width, and typical properties of 2500 kg/m^3 unit weight, 3.5x10^{10} kN/m^2 modulus of elasticity in the longitudinal direction, 3.22x10^{10} kN/m^2 in the transverse direction and 0.2 Poisson's ratio. Bridge damping is considered to be null. The first natural frequencies of the bridge are 5.02 (longitudinal), 15.08 (torsional), 20.00 (longitudinal) and 34.42 (torsional) Hz.

A rigid two-axle trailer model is used for the simulations. The FE truck and bridge models are represented in Figure 1. The axle spacing for the two-axle truck is 5.5 m and the distance between wheels of an axle is 2 m. The total front and rear static axle weights are 59.5 and 108.6 kN respectively. The inner wheels of the two-axle truck are driven at 0.5 m from the bridge centerline as represented in Figure 2. This 3-D truck model is composed of bar, mass, damping, spring and rigid elements making up the tire, suspension, frame and body mass of the vehicle. The data for the dynamic parameters of the truck has been taken from manufacturers [29,30]: tire and suspension damping are 3,000 and 5,000 N·s/m respectively, tire and suspension stiffness are taken as 1,000,000 N/m, the body mass is 16,500 kg and the corresponding pitching moment of inertia is 425,000 kg·m^2. The first modes of vibration of the truck are frame twist (0.15 Hz), body pitch (1.07 Hz), body bounce (2.08 Hz) and axle hop out of phase (16.36 Hz). Three speeds (20, 25 and 30 m/s) have been employed in the simulations.

The road profile has been generated stochastically from power spectral density functions following guidelines by ISO standards [31,32]. Two types of road profile have

been considered: ‘smooth’ and ‘rough’ with geometric spatial means of $4x10^{-6}$ m^3/cycle and $32x10^{-6}$ m^3/cycle respectively.

Bridge strains, which are easily measurable in the field, are obtained at 21 bridge locations and contaminated with Gaussian noise. The strains are located at 3 longitudinal sections (quarter, mid and three quarter span) and 7 transverse measurements equally spaced across the section width. The 2% noise is added to the theoretical strains as a normally distributed variable of zero mean and standard deviation 2% of the maximum strain. Figure 3 shows the simulated noise-free and noisy strain at one the midspan locations, as the truck crosses the bridge over the smooth surface at 20 m/s. It is the noisy data that will be used for testing the MFI B-WIM algorithm presented in the following sections. Then, forces will be estimated using MFI and compared to the ‘true’ applied forces.

3. MOVING FORCE IDENTIFICATION THEORY

The solution to the MFI problem involves four main steps:

1. Conversion of the equilibrium equation of motion to a vector matrix differential equation suitable for dynamic programming.
2. Formulation of the inverse problem as a least squares minimization with Tikhonov regularization.
3. Use of dynamic programming which provides an efficient solution to the problem.

4. Solving for the optimal regularization parameter using Hansen's L-curve method.

In the above procedure, it is assumed that vehicle velocity, number of axles and axle spacings are known, i.e., from axle detectors on the road, and that changes in the bridge stiffness and mass matrices are negligible with the passage of the vehicle.

3.1. Inverse model and state space equations

The MFI problem requires a mathematical model that accurately represents the physical properties of the bridge. A FE formulation has been chosen as it is deemed to be the most versatile in problems of this nature. The method of dynamic programming requires the equilibrium equation of motion to be converted into a discrete system. In this case, the motion of the dynamic bridge model is defined by Equation (1).

$$\left[M_g\right]_{nxn}\left\{\ddot{y}\right\}_{nx1}+\left[C_g\right]_{nxn}\{\dot{y}\}_{nx1}+\left[K_g\right]_{nxn}\left\{y\right\}_{nx1}=[L(t)]_{nxn_g}\left\{g(t)\right\}_{n_g x1} \quad (1)$$

where $[L(t)]$ is a time varying location matrix relating the n_g applied vehicle forces of the vector $g(t)$ to the n degrees of freedom (DOF's) of the model. $[M_g]$, $[C_g]$ and $[K_g]$ are the global mass, damping and stiffness matrices respectively. $\{\ddot{y}\}$ are nodal accelerations, $\{\dot{y}\}$, nodal velocities, and $\{y\}$, nodal displacements. The storage requirements of the dynamic programming routine for system of Equations (1) are very expensive, and some technique is necessary to reduce the dimension of the system. An eigenvalue reduction technique is employed for this purpose [24,33]. It is assumed that

the displacements vector, $\{y\}$, can be replaced with an equivalent vector of modal coordinates, $\{z\}$, through Equation (2).

$$\{y\} = [\Phi]_{nxn_z} \{z\}_{n_z x1} \tag{2}$$

where $[\Phi]$ is the modal matrix of normalized eigenvectors and n_z is the number of modes [34,35]. By replacing Equation (2) into (1) and performing the required manipulations, Equation (1) can be re-written as the decoupled set of equations expressed by Equation (3).

$$[I]_{nxn} \{\ddot{z}\}_{nx1} + 2\zeta [\Omega]_{nxn} \{\dot{z}\}_{nx1} + [\Omega]_{nxn} \{z\}_{nx1} = [\Phi]^T [L(t)]_{nxn_g} \{g(t)\}_{n_g x1} \tag{3}$$

where $[\Omega]$ is a diagonal matrix containing the natural frequencies and ζ is the percentage damping. Equation (3) can now be formulated as a vector matrix differential equation where the state vector $\{X\}$ is defined by Equation (4).

$$\{X\}_{2nx1} = \begin{Bmatrix} z \\ \dot{z} \end{Bmatrix} \tag{4}$$

By combining Equations (3) and (4) [23,36], it is possible to obtain the vector matrix differential Equation (5).

$$\left\{\frac{dX}{dt}\right\}_{2\text{nx}1} = \left[\text{A}\right]_{2nx2n}\{X\}_{2\text{nx}1} + [\text{B}]\{\text{g}\}_{n_g x1} \tag{5}$$

where [A] and [B] are defined by Equations (6) and (7) respectively.

$$[A] = \begin{pmatrix} 0 & I \\ -[\Omega] & -2\zeta[\Omega] \end{pmatrix} \tag{6}$$

$$[B] = \begin{pmatrix} 0 \\ [\Phi]^T \left[L(t)\right] \end{pmatrix} \tag{7}$$

The continuous system of differential equations can be converted into a direct integration scheme, often referred to as a zeroth order system [24] defined by,

$$\{X\}_{j+1} = [M]\{X\}_j + [P]_j\{g\}_j \tag{8}$$

Where, [M] = exp([A]*h), h is the time step, N is the total number of discrete measurements and $[P]_j$ is defined by Equation (9).

$$[P]_j = [[A]^{-1}[[M]-[I]]]\begin{bmatrix} 0 \\ [\Phi]^T[L]_j \end{bmatrix} \tag{9}$$

However it has been shown [24,37], that by converting equation (8) into a first order system where the forces to be predicted are included in the state vector and it is the

derivative of the force that is regularised for, results in a smoother and more accurate solution. The first order system is defined by Equation (10)

$$\begin{Bmatrix} X \\ g \end{Bmatrix}_{j+1} = \begin{bmatrix} [M] & [P]_j \\ 0 & [I] \end{bmatrix} \begin{Bmatrix} X \\ g \end{Bmatrix}_j + \begin{Bmatrix} [0] \\ [I] \end{Bmatrix} \{r\}_j \qquad j = 1,2,\ldots N$$
$$\begin{Bmatrix} X \\ g \end{Bmatrix}_{j+1} = [K]_j \begin{Bmatrix} X \\ g \end{Bmatrix}_j + [T]\{r\}_j \qquad (10)$$

3.2. Least squares and dynamic programming

In B-WIM, the measurements taken on the bridge are usually strains and not the state variables themselves. In order to formulate the problem as a least squares minimisation, the theoretical strains, $\{\varepsilon^{th}\}$, must be related to the state variables, {X}. This can be achieved through a [*Q*] matrix which is generally some form of a finite difference scheme related to the strain displacement matrix of the individual finite element used. So, the relationship vector of strains to state variables at a particular time step is obtained via Equation (11).

$$\left\{\varepsilon^{th}\right\}_{\text{mx1}} = \left[\text{Q}\right]_{mx2n} \{X\}_{\text{2nx1}} \qquad (11)$$

where *m* is the number of simultaneous strain measurements. Since a finite number of modes are used in the analysis, this relationship is redefined as Equation (12).

$$\{\varepsilon^{th}\}_j = [Q]\begin{pmatrix} [\Phi] & 0 & 0 \\ 0 & [\Phi] & 0 \\ 0 & 0 & 0 \end{pmatrix}\begin{Bmatrix} X \\ g \end{Bmatrix}_j \qquad j = 1,2,\ldots..,N \qquad (12)$$

The problem is now formulated as a least squares minimisation with Tikhonov regularization as given by Equation (13).

$$E(X_j, r_j) = \sum_{j=1}^{m}\left(\left\{\{\varepsilon^{me}\}_j - [Q]\{X\}_j\right\},\ [W]\left\{\{\varepsilon^{me}\}_j - [Q]\{X\}_j\right\} + \{r\}_j\ ,[B]\{r\}_j\right) \qquad (13)$$

Where $\{\varepsilon^{me}\}$ is the vector of measured strain, (x,y) denotes the vector product of x and y, $[W]$ is an $m \times m$ identity matrix in the least squares error, and $[B]$ is an $n_g \times n_g$ diagonal matrix containing the optimal regularization parameter b. The regularisation term is added to provide bounds to the error in the ill-conditioned least squares formulation and also to control the amount of smoothness in the solution.

In order to solve Equation (13), it is necessary to calculate the optimal derivative of the forces that cause the system to best match the given measurements $\{\varepsilon\}$ for an optimal regularization parameter b. This minimization problem can be solved using Bellman's principle of optimality [38,39]. So, Equation (14) is the result of applying the principle of optimality to Equation (13).

$$f_{j-1}(X) = \min_{r_{j-1}}\left\{\left\{\varepsilon^{me}\right\}_{j-1} - [Q]\{X\}_{j-1}\right\},\ [W]\left\{\left\{\varepsilon^{me}\right\}_{j-1} - [Q]\{X\}_{j-1}\right\} + \{r\}_{j-1}, [B]\{r\}_{j-1} + f_j\left\{[K]_{j-1}\{X\}_{j-1} + [T]\{r\}_{j-1}\right.$$

(14)

where f is the optimal cost for each time step, $\{r\}$ is the optimal derivative of the force, and matrices $[K]$ and $[T]$ are defined in Equation (10). The minimum $E(X,r)$ at each point is determined by selecting the forcing function $\{\underline{r}\}_{j-1}$ that minimizes f_{j-1}. This function can be written in quadratic form in terms of $\{X\}$ as Equation (14).

$$f_j(X) = (\{X\}, [R]_j \{X\}) + (\{s\}_j, \{X\}) + q_j \tag{15}$$

By equating like terms of X in Equations (14) and (15), recurrence equations can be derived for both $[R]_j$ and $\{s\}_j$ [24,25]. These equations and additional terms are described in Appendix A

3.3. L-curve and optimal initial conditions

Previous studies in MFI have shown that the L-curve is an efficient and accurate method to calculate the optimal regularization parameter [37]. The L-curve is a plot of the solution norm (F_{norm}) versus the residual least squares norm (E_{norm}) with the optimal regularization parameter located at the corner of the L-curve. For the first order regularization the norms that are plotted are defined as:

$$E_{norm} = \sqrt{\sum_{j=1}^{m} \left(\left\{ \{\varepsilon^{me}\}_j - [Q]\{X\}_j \right\}, [W] \left\{ \{\varepsilon^{me}\}_j - [Q]\{X\}_j \right\} \right)} \tag{16}$$

$$F_{norm} = \sqrt{\sum_{j=1}^{m} \left(r_j, r_j \right)} \tag{17}$$

The optimal regularization parameter is located at the corner of the L-curve, at the point of maximum curvature [40]. Once the optimal regularization parameter has been obtained from the L-curve, the solution to the MFI problem can be further improved by applying optimal initial conditions on the state vector at certain time instances. There are two stages involved in the dynamic programming routine: a backward and a forward sweep. Once all of the terms in the backward sweep have been determined, the forward sweep is defined by Equations (18) and (19).

$$\{r\}_{j-1} = -[D]_j [T]^T \{s\}_j - [D]_j [H]_j [K]_{j-1} \begin{Bmatrix} X_{j-1} \\ g_{j-1} \end{Bmatrix} \tag{18}$$

$$\begin{Bmatrix} X_j \\ g_j \end{Bmatrix} = [K]_{j-1} \begin{Bmatrix} X_{j-1} \\ g_{j-1} \end{Bmatrix} + [T]\{r\}_{j-1} \tag{19}$$

where [*D*] and [*H*] are defined in Appendix A

The optimal initial condition for the state vector can be found by minimizing Equation (15) with respect to the state vector [19], which results into Equation (20).

$$\begin{Bmatrix} X_1 \\ g_1 \end{Bmatrix}^* = -[R_1]^{-1} \{s_1\} / 2 \tag{20}$$

where * denotes the optimal. This gives optimal initial condition for the wheel forces and also the displacements and velocities of the DOF's if the bridge was not at rest. Furthermore, the solution can be greatly improved by implementing known boundary conditions on the $\{g_j\}$ terms of the state vector. For example, when there is only one axle on the bridge, the terms in the vector of forces, $\{g\}$, corresponding to the second axle are zerod for each iteration of the forward sweep, and at the instance the second axle enters the bridge, the term in the vector of forces corresponding to that axle are initialized with the initial condition $\{g_1\}$.

4. TESTING WITH SIMULATED MEASUREMENTS

The MFI B-WIM algorithm described in the previous section has been coded with MATLAB software [41] and it is tested using an independent VBI model built with MSc/NASTRAN software (Figure 1). Noisy measurements have been simulations at a number of locations for a two-axle vehicle passing over a bridge as described in Section 2. Then, individual wheel forces have been estimated from these noisy measurements using the MFI B-WIM MATLAB program. Finally, individual wheel forces have been added together to obtain the axle force for each instant in time.

First of all, the MFI algorithm requires a theoretical model of the bridge. An orthotropic C1 conforming plate bending element [42,43] is used to model the simply supported bridge described in Section 2. The element is a four node rectangle with 4 DOF's per node: displacement, rotation about the x axis, rotation about y axis, and nodal twist which ensures inter element slope compatibility. The FE mesh is generated such that the

wheels are moving along the nodal lines of the mesh. The bridge model is discretized into 720 square plates each of size 0.5 *x* 0.5 m. The total number of DOF's is $n = 3116$ and the number of unknown wheel forces is $n_g = 4$. Unless otherwise specified, 25 mode shapes, with a frequency range from 5 to 305 Hz, and 8 measurement locations (2 at ¼ span, 4 at midspan and 2 at ¾ span) are employed in the analysis ($m = 8$ and $n_z = 25$).

Figure 4 shows the L-curve when the vehicle travels at 30 m/s on the smooth profile. From this curve, an optimal *b* parameter of 3e-16 is obtained. The 'true' and the 'predicted by the MFI B-WIM algorithm' axle force histories, are represented by continuous and dashed lines respectively in Figure 5. The road profile is very smooth and the vehicle dynamics are small. There is only a main low frequency that the MFI algorithm is able to model for both axles accurately. When driving the vehicle at 30 m/s over a rough profile, the L-curve provides an optimal parameter of b = 1e-18 and the axle force history is illustrated in Figure 6. In the latter, there are two dominant axle frequencies and a clear correspondence between predicted (dashed) and simulated (continuous) instantaneous axle forces can be found. Although some peaks are missed, the average value about which dynamics oscillates is very similar for 'true' and predicted axle forces. As expected, values are inaccurate at both ends of the instantaneous calculation as result of the small contribution to the total strain of an axle just entering or leaving the bridge. Figure 7 shows the force history for the 30 m/s run over a rough profile when using 21 measurement locations and 25 modes, with a frequency range from 5Hz to 543Hz (an optimal parameter b = 5e-17 was found to give best results according to the corresponding L-curve). It can be seen there is hardly any improvement comparing it to Figure 6 based on only 8 sensors and 25 mode shapes.

The algorithm didn't give satisfactory results below 8 sensors for of the 4 unknown wheel forces and 20 m bridge being tested. Figures 8 and 9 show the corresponding time-axle forces histories when the vehicle travels at 25 m/s for the two road roughness under consideration. These histories are derived using optimal *b* parameters of 1e-16 and 5e-17 for the smooth and rough profiles respectively. Again, the MFI algorithm is able to accurately model the axle forces for the smooth profile and it is able to catch the two main frequencies for the rough profile. In the latter, the algorithm fails to accurately predict the amplitude of the axle dynamics, in particular those cases where there is a pronounced peak at a high frequency. Figure 10 and 11 show the results for the runs at 20 m/s and the same conclusions arise. In addition to the axle force history, Figure 11 includes the 'true' and predicted force history for the left wheel of the front axle.

Table 1 compares the error (%) in the prediction of static weights for both axles and Gross Vehicle Weight (GVW) using the traditional B-WIM static algorithm [2] and the MFI approach. For the MFI solution, the static weight is obtained from the average of the predicted force history. B-WIM accuracy classifications are commonly based on mean and standard deviations of a number of truck crossings. Although the mean error is relatively low by both algorithms, the MFI solution provides a clear lower standard deviation of all truck crossings (standard deviations in front and rear axle of 12 and 8.27 respectively by traditional WIM compared to 4.8 –front– and 2.27 –rear– by MFI). The improvement is more significant in individual axle weights, since the traditional B-WIM algorithms tends to compensate errors in front and rear axles when added together to calculate the GVW (standard deviation in GVW of 2.37 and 1.73 by traditional B-WIM and MFI algorithms respectively) .

5. ERROR STUDIES

The model outlined in Section 2 is considered here again but subject to the following forcing functions traveling at 20m/s along the path previously defined:

$$
\begin{aligned}
W_1(t) &= 35,000(1+.1\sin(3\pi t)+.1\sin(5\pi t)+.05\sin(25\pi t)+.05\sin(30\pi t)\\
W_2(t) &= 35,000(1+.1\sin(3\pi t)+.1\sin(5\pi t)+.05\sin(25\pi t)-.05\sin(30\pi t)\\
W_3(t) &= 50,000(1-.1\sin(3\pi t)+.1\sin(5\pi t)-.05\sin(25\pi t)-.05\sin(30\pi t)\\
W_4(t) &= 50,000(1-.1\sin(3\pi t)+.1\sin(5\pi t)-.05\sin(25\pi t)+.05\sin(30\pi t)
\end{aligned}
\tag{21}
$$

It is assumed $W_1(t)$ and $W_2(t)$ represent the wheel forces of a front axle while $W_3(t)$ and $W_4(t)$ simulate the wheel forces of a rear axle. The strains at 21 locations on the bridge are simulated using the full stiffness and mass matrices, using a Newmark Beta direct integration scheme. The model is remeshed, using 20 elements along the x-axis and 9 along the y-axis giving a total of 180 elements, 210 nodes and 840 degrees of freedom. The model is remeshed for the purpose of simulation only; the inverse model employed is the same as defined in Section 3.1. Noise is added to the simulated strain in all cases; the noise added to all 'measurements', it is 2% unless otherwise specified. This magnitude of noise has been added as it is deemed to be comparable to relative signal to noise ratios (RSNR) encountered in the field of approximately 8%. The number of modes used in all cases is 25. Several parameters are analyzed for their effect on the accuracy of the MFI algorithm. In the following subsections, the error in identified forces are calculated as defined by [15,16]:

$$
Error = \frac{\| F_{true} - F_{identified} \|}{\| F_{identified} \|} \times 100 \tag{22}
$$

where $\|.\|$ denotes the Euclidean norm of the vector, and F_{true} and $F_{identified}$ are the true and identified forces respectively.

5.1 Effect of noise

The noise is added to the simulated strain at each 'measurement' location as a product of the maximum strain. The noise is added in this manner as it is assumed that the nature of the noise measured in the field would be of a similar magnitude across all sensors. In total six levels of noise are analysed for their effect on the accuracy of the MFI algorithm. Table 2 shows the percentage errors in identified forces for each of the noise levels used in the study. It can be seen that, in general, the errors in the identified forces increase in proportion to the percentage of noise. However it should be noted that even in the case of 10% noise, where the RSNR is upwards of 30%, the percentage error in the identified axle forces is only 8.1% and 8.3% for axles 1 and 2 respectively, using 21 'measurement' locations. Figure 12 shows the theoretical and identified forces for W_1 and '$W_1 + W_2$' for the case of 20 m/s and 3% noise added to the simulated strain. It can be seen from this figure that again excellent results are achieved for both the axle load history and the individual wheel load; both the magnitude and main truck frequency are identified in both cases. However the higher truck frequencies are not accurately identified.

5.2 Effect of velocity

The effect of vehicle velocity on the accuracy of the MFI algorithm is analyzed for the scenario detailed above. The velocity is varied from 10 m/s to 40 m/s in increments of 5. The errors in identified forces with respect to vehicle velocity are shown in Table 3.

In general it was found that the MFI algorithm is predominately independent of the velocity with maximum and minimum errors of approximately 7.5 and 4% respectively.

5.3 Effect of transverse location of the forces

The effect of the transverse location of the forces on the accuracy of the MFI algorithm is analyzed for the same scenario. The transverse location is varied from a point where 1 is then shifted transversely in increments of 1 m to 4 m while keeping the relative spacing between wheels fixed (Figure 13). After this point it is assumed that the response of the bridge is symmetrical and further iteration is not necessary. Table 4 shows the errors in the identified forces versus the transverse position of the forces for 21 'measurement' locations. In all scenarios where 21 measurements are used, the % errors in identified forces are approximately equal.

6. CONCLUSIONS

The application of optimization techniques to minimize errors in axle spacings and speed have improved the accuracy of static B-WIM algorithms noticeably. However, noise and the dynamic excitation of the bridge have remained as very important sources of error. The latter will depend on the truck mechanical characteristics and the conditions of the road prior to and on the bridge. So, rough road profiles generally result in very poor accuracy of individual axle weights by the traditional static B-WIM algorithm. This paper has presented a B-WIM algorithm based on MFI theory that minimizes inaccuracies due to both noise and dynamics. This algorithm requires the monitoring of the bridge deformation at a number of sensor locations (in excess of the number of vehicle forces) and an accurate theoretical model of the bridge response.

Then, inverse programming and Tikhonov regularization are applied to the theoretical bridge model and to the bridge measurements to derive the optimal force solution.

B-WIM systems normally add all strains measurements available at each longitudinal location to compensate for the deviations introduced by different truck transverse positions. However, the bridge bends more at some particular transverse locations and the added strain is also bigger. As a further improvement, the B-WIM algorithm presented in the paper has taken into consideration the truck transverse location. In practice, this transverse location can be determined with the use of three axle detectors: two perpendicular to the traffic flow and a third one at an angle. Nevertheless, B-WIM systems are still limited to short and medium span bridges since very long span bridges would require an excessive number of sensors and it would be difficult to exactly locate the truck at each instant.

The multiple-sensor B-WIM algorithm based on MFI theory has been tested with independent MSc/NASTRAN FE software that simulated the passage of a two-axle vehicle over a bridge with two types of road roughness at different speeds. Noise has been added to the results of the VBI simulations. It has been shown how such an algorithm can be employed to gather more and better B-WIM data than a simple static approach. So, the static value or average value of the axle forces about which dynamics oscillate can be more accurately calculated since noise and dynamics are removed safely. An indication of the main frequencies of vibration of an axle on the bridge can also be obtained, although the exact amplitude of these dynamics is difficult to predict.

APPENDIX A

The first order system of Equation (10) is rewritten as,

$$\{\hat{X}\}_{j+1} = [K]_j \{\hat{X}\}_j + [T]\{r\}_j$$

where,

$$\{\hat{X}\}_j = \begin{Bmatrix} X_j \\ g_j \end{Bmatrix}$$

Recurrence relations for the first order regularization

$$E(\hat{X}, r_j) = \sum_{j=1}^{N} (\{\varepsilon^{me}\}_j - [Q]\{\hat{X}\}), [W](\{\varepsilon^{me}\}_j - [Q]\{\hat{X}\}) + \{r\}_j, [B]\{r\}_j$$

$$f_{j-1}(\hat{X}) = \min_{r_{j-1}} ([Q]\{\hat{X}\} - \{\varepsilon^{me}\}_{n-1}, [W]([Q]\{\hat{X}\} - \{\varepsilon^{me}\}_{n-1})) + \{r\}_{j-1}, [B]\{r\}_{j-1} + f_j([K]_{j-1}\{\hat{X}\} + [T]\{r\}_{j-1})$$

(A1)

The initial conditions for the backward sweep are given by $j = N$ and:

$$\begin{aligned} [R]_N &= [Q]^T [W][Q] \\ \{s\}_N &= -2[Q]^T [W]\{\varepsilon^{me}\}_N \\ q_N &= (\{\varepsilon^{me}\}_N, [W]\{\varepsilon^{me}\}_N) \end{aligned} \tag{A2}$$

In the backward sweep, the following relationships are employed

$$\begin{aligned} [H]_j &= 2[T]^T [R]_j \\ [D]_j &= [2[B] + 2[T]^T [R]_j [T]]^{-1} \end{aligned} \tag{A3}$$

Using the equations above the Riccati recurrence equations can be defined by

$$\begin{aligned}[R]_{j-1} &= [Q]^T [W][Q] + [K]_{j-1}^T ([R]_j - [H]_j^T [D]_j [H]_j / 2)[K]_{j-1} \\ \{s\}_{j-1} &= -2[Q]^T [W]\{\varepsilon^{me}\}_{j-1} + [K]_j^T ([I] - [H]_j^T [D]_j [H]_j)\{s\}_j\end{aligned} \tag{A4}$$

And finally, for $j = 1$ to N the forward sweep is defined by

$$\begin{aligned}\{\hat{X}\}_j &= [K_{j-1}]\{\hat{X}\}_{j-1} + [T]\{r\}_{j-1} \\ \{r\}_j &= -[D]_{j+1}[T]^T \{s\}_{j+1} - [D]_{j+1}[H]_{j+1}[K]_{j+1}\{\hat{X}\}_j\end{aligned} \tag{A5}$$

REFERENCES

1. Brozovič R, Vodopivec V, Žnidarič A. Slovenian experience of using WIM data for road planning and maintenance. *Proceedings of Fourth International Conference on Weigh-In-Motion (ICWIM4)* 2005, Taipei, Taiwan, February; 363-370.
2. Moses F. Weigh-In-Motion system using instrumented bridges. *ASCE Transportation Engineering Journal* 1979; **105**: 233-249.
3. O'Brien EJ, Žnidaric A, Dempsey AT. Comparison of two independently developed Bridge Weigh-In-Motion systems. *Heavy Vehicle Systems, Int. J. of Vehicle Design* 1999; 6(1/4):147-162.

4. González A. Development of Accurate Methods of Weighing Trucks in .Motion. PhD Thesis. Department of Civil Engineering, Trinity College, Dublin, Ireland, 2001.
5. O'Conor C, Chan THT. Dynamic wheel loads from bridge strains. *ASCE Journal of Structural Engineering* 1988; **114**:1703-1723.
6. Zhu XQ, Law SS. Orthogonal function in moving loads identification on a multi-span bridge. *Journal of Sound and Vibration* 2001; **252(2)**:329-345.
7. Law SS, Bu JQ, Zhu XQ, Chan SL. Vehicle axle loads identification using finite element method. *Engineering Structures* 2004; **26**: 143-1153.
8. Chan THT, Yung TH. A theoretical study of force identification using prestressed concrete bridges. *Engineering Structures* 2000; **23**:1529-1537.
9. Law SS, Chan THT, Zeng QH., Moving force identification: A time domain method. *Journal of Sound and Vibration* 1997; **201**:1-22
10. Law SS, Chan THT, Zeng QH. Moving force identification: a frequency and time domain analysis. *ASME Journal of Dynamic systems, Measurement and Control* 1999; **12**:394-401.
11. Yu L, Chan THT. Moving force identification based on the frequency-time domian method. *Journal of Sound and Vibration* 2003; **261**:329-349.
12. Chan THT, Law SS, Yung TH. An interpretive method for moving force identification. *Journal of sound and vibration* 1999; **219**(3):503-524.
13. Yu L, Chan THT. Identification of Multi-axle vehicle loads on bridges. *ASME Journal of vibration and acoustics* 2003; **126**: 17-26.
14. Tikhonov AN, Arsenin VY. *Solutions of ill-posed problems.* New York: John Wiley & sons, 1977.

15. Zhu XQ, Law SS. Moving loads identification through regularization. *ASCE Journal of Engineering Mechanics* 2002; **128**(9):989-1000.
16. Law SS, Chan THT, Zhu XQ, Zeng QH. Regularization in Moving force Identification. *ASCE Journal Engineering Mechanics* 2001; **127**(2):136-148.
17. Zhu XQ, Law SS. Identification of moving interaction forces with incomplete velocity information. *Mechanical Systems and Signal Processing* 2003;**17**(6):1349-1366.
18. Zhu XQ, Law SS. Moving forces identification on a multi-span continuous bridge., *Journal of sound and vibration* 1999; **228**(2):377-396.
19. Law SS, Zhu XQ. Study on different beam models on moving force identification. *Journal of sound and vibration* 2000; **234**(4):661-679.
20. Zhu XQ, Law SS. Moving load identification on multi-span continuous bridges with elastic bearings. *Mechanical Systems and Signal Processing*, 2006: **20:** 1759-1782
21. Zhu XQ, Law SS. Identification of vehicle axle loads from bridge dynamic responses. *Journal of sound and vibration* 2000; **236**(4):705-724.
22. Zhu XQ, Law SS. Identification of moving loads on an orthotropic plate. *Journal of vibration and acoustics* 2001; **123**:238-244.
23. Zhu XQ, Law SS. Time domain identification of moving loads on bridge deck. *Journal of vibration and acoustics* 2003; **125**:187 –198.
24. Trujillo DM, Busby HR. *Practical Inverse Analysis Engineering*, New York: CRC Press, 1997.
25. Trujillo DM. Application of dynamic programming to the general inverse problem. *International Journal for Numerical Methods in Engineering* 1977; **12**:613-624.

26. Law SS, Fang YL. Moving force identification: optimal state estimation approach. *Journal of Sound and Vibration* 2001; **239**(2):233-254.

27. The MacNeal-Schwendler Corporation, *MSC/NASTRAN for Windows, Command Reference Guide.* USA, 1997

28. Cifuentes AO. Dynamic response of a beam excited by a moving mass. *Finite Elements in Analysis and Design 5* 1989; 237-246.

29. Baumgärtner W. Bridge-Vehicle Interaction using extended FE analysis. *Heavy Vehicle Systems, Int. Journal of Vehicle Design* 1999; **6**(1-4):1–12.

30. Kirkegaard PH, Nielsen SRK, Enevoldsen I. Heavy vehicles on minor highway bridges – Dynamic modelling of vehicles and bridges. Report in Department of Building technology any and Structural Engineering, Aalborg University, ISSN 1395-7953 R9721, December, 1997.

31. ISO 8608:1995. *Mechanical Vibration-Road Surface Profiles-Reporting of Measured Data*. International Standards Organisation, 1995.

32. Wong JY. *Theory of Road Vehicles*. John Wiley and Sons, 1993.

33. Busby HR, Trujillo DM. Solution of an inverse dynamics problem using an eigenvalue reduction technique. *Computers and Structures* 1986; **25**:109-117.

34. Craig R. *Structural Dynamics an Introduction to Computer Methods*. John Wiley and Sons, 1981.

35. Clough R, Penzien S. *Dynamics of Structures*, McGraw Hill, New York, 1978.

36. Trujillo DM. The direct numerical integration for linear matrix differential equations using Pade approximations. *International Journal for Numerical Methods in Engineering* 1975; **9**:259-270.

37. Busby HR, Trujillo DM. Optimal regularization of an inverse dynamics problem. *Computers and Structures* 1995; **63**:243-248.
38. Bellman R. *Introduction to Mathematical Theory of Control Process, Volume I*. New York: Academic Press, 1965.
39. Bellman R. *Introduction to Mathematical Theory of Control Process, Volume II*. New York: Academic Press, 1965.
40. Hansen PC. Analysis of discrete ill-posed problems by means of the L-curve. *SIAM Review* 1992*;* **34**(4):561-580.
41. The MathWorks, Inc. *Matlab, theLanguage of Technical Computing, version 6.0*, 2000.
42. Bogner FK, Fox RL, Schmit LA. The generation of inter-element-compatible stiffness and mass matrices by the use of interpolation formulas. *Proceeding's of the 1st conference on matrix methods in structural mechanics* 1965. Air Force Inst of Tech, Wright Patterson A.F. Base, Ohio, 397-443.
43. Zienkiewicz OC. *The Finite Element Method in Engineering Science*. McGraw-Hill, New York, 1977.

LIST OF TABLES

		% Error by traditional BWIM			% Error by MFI solution		
Velocity	**Road**	**Axle 1**	**Axle 2**	**GVW**	**Axle 1**	**Axle 2**	**GVW**
20	good	8.07	-2.50	1.24	-0.17	-0.96	-0.68
20	poor	5.30	-8.66	-3.72	-4.15	-3.98	-4.04
25	good	8.03	-0.92	2.25	-0.93	0.01	-0.32
25	poor	13.67	-4.41	1.99	-12.36	2.10	-3.02
30	good	0.77	1.90	1.50	0.59	0.00	0.21
30	poor	-20.35	15.39	2.74	-4.95	2.18	-0.34

Table 1 – Percentage errors in the predicted static weight by traditional BWIM algorithm and by MFI solution

Percentage Noise	W1 % Error	W2 % Error	W3 % Error	W4 % Error	Axle 1 % Error	Axle 2 % Error
1	5.7	6.5	6.3	6.0	4.7	4.5
2	5.6	6.4	6.2	6.0	4.8	4.5
3	5.8	6.5	6.4	6.2	5.0	4.7
4	5.9	6.0	6.2	6.0	5.0	4.9
5	6.2	6.5	6.7	6.9	5.6	5.6
10	8.9	8.4	9.1	8.6	8.1	8.3

Table 2 – Percentage error in the predicted forces for a number of noise levels

Velocity m/s	W1 % Error	W2 % Error	W3 % Error	W4 % Error	Axle 1 % Error	Axle 2 % Error
10	5.7	6.0	6.0	6.3	5.0	4.8
15	7.4	6.5	7.3	7.5	6.3	6.6
20	5.6	6.3	6.1	5.8	4.4	4.1
25	6.8	6.3	6.3	6.0	5.5	5.0
30	3.7	4.9	5.6	5.9	3.5	4.1
35	4.1	4.9	6.0	6.6	4.2	5.0
40	6.1	5.4	6.0	5.4	4.9	4.9

Table 3 – Errors in the identified forces versus vehicle velocity using 21 'measurement' locations

Transverse Position W1	W1 % Error	W2 % Error	W3 % Error	W4 % Error	Axle 1 % Error	Axle 2 % Error
0	5.4	6.0	6.2	5.8	4.5	4.4
1	5.4	6.6	6.3	6.1	4.3	4.1
2	5.6	6.3	6.1	5.8	4.4	4.1
3	5.8	5.5	5.6	5.6	4.7	4.4
4	5.8	5.5	5.8	5.6	4.7	4.5

Table 4 – Percentage errors in the identified forces for a number of transverse positions of the moving forces

LIST OF FIGURES

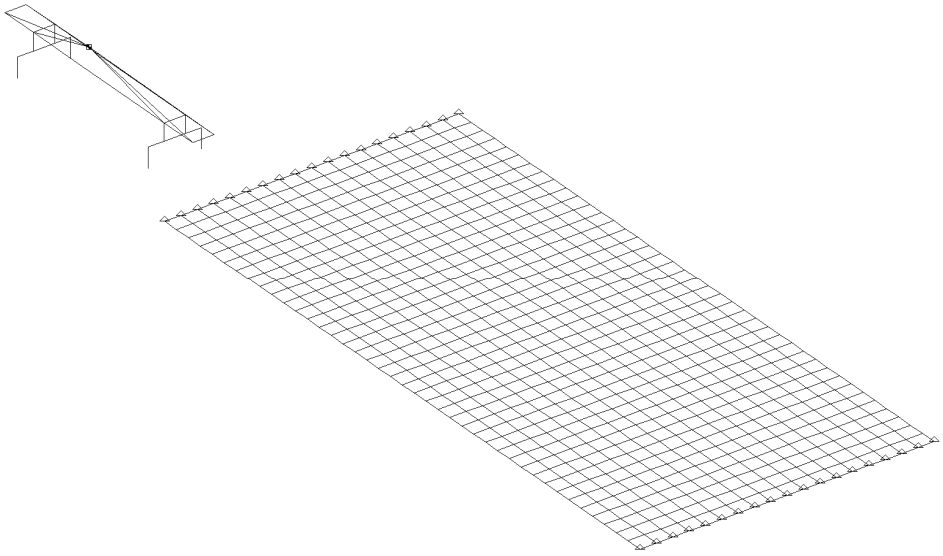

Figure 1

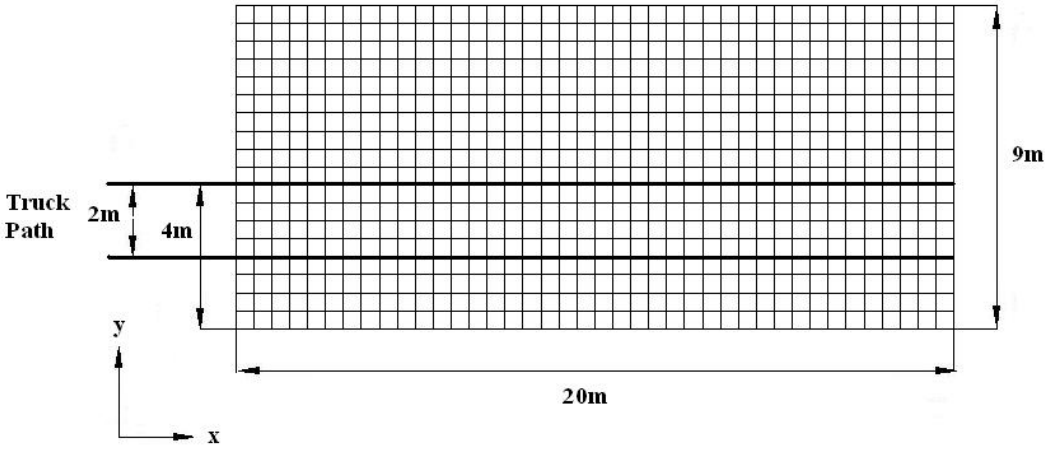

Figure 2

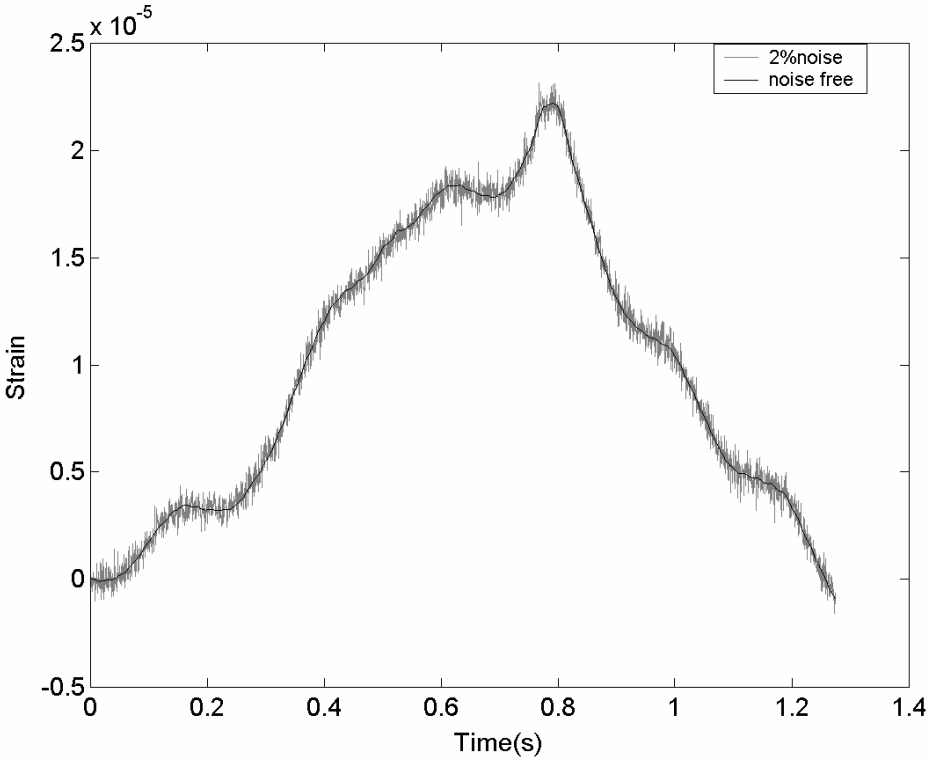
x 10^-5
2.5
2
1.5
1
0.5
0
-0.5
Strain
0
0.2
0.4
0.6
0.8
1
1.2
1.4
Time(s)
2%noise
noise free

Figure 3

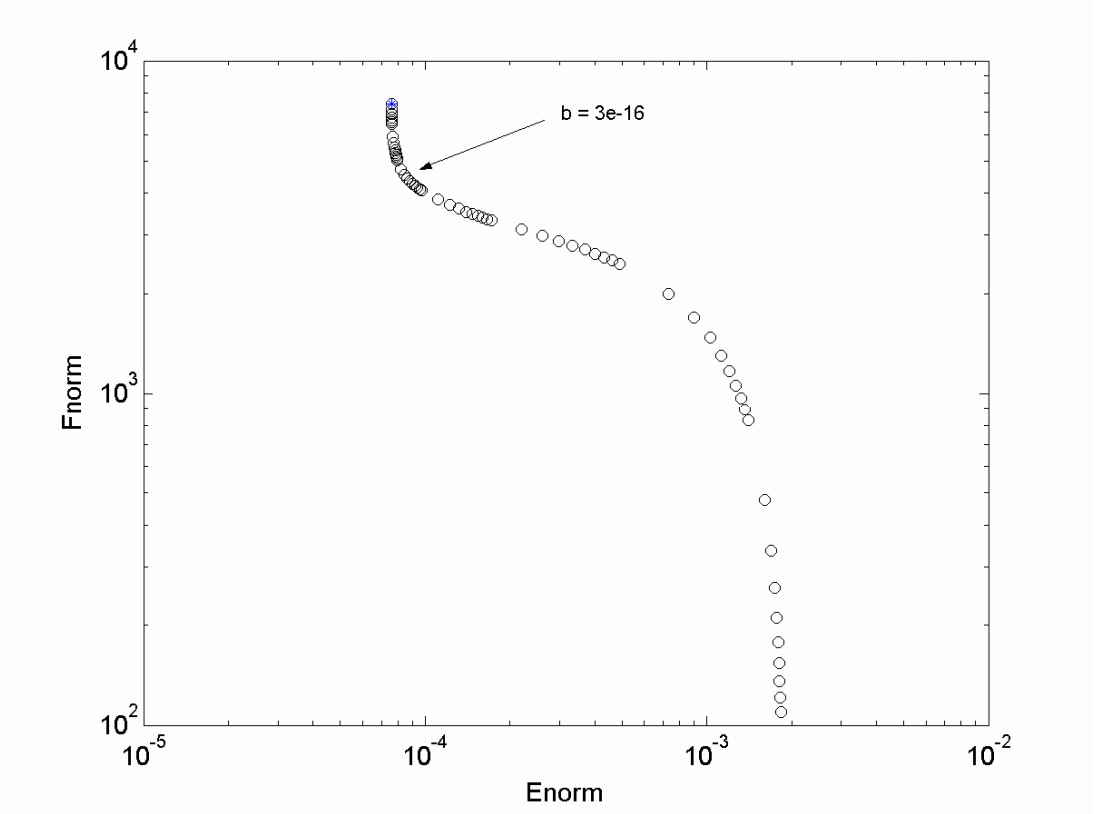

Figure 4

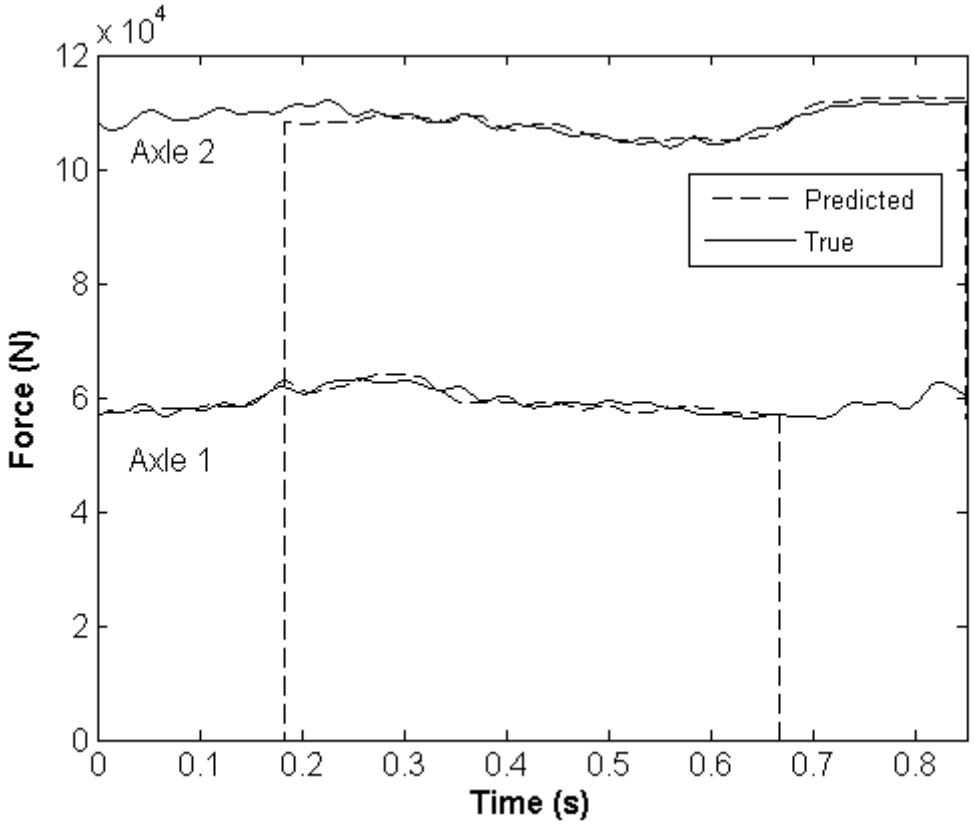
x 10^4
12
10
8
6
4
2
0
Force (N)
Axle 2
Axle 1
Predicted
True
0
0.1
0.2
0.3
0.4
0.5
0.6
0.7
0.8
Time (s)

Figure 5

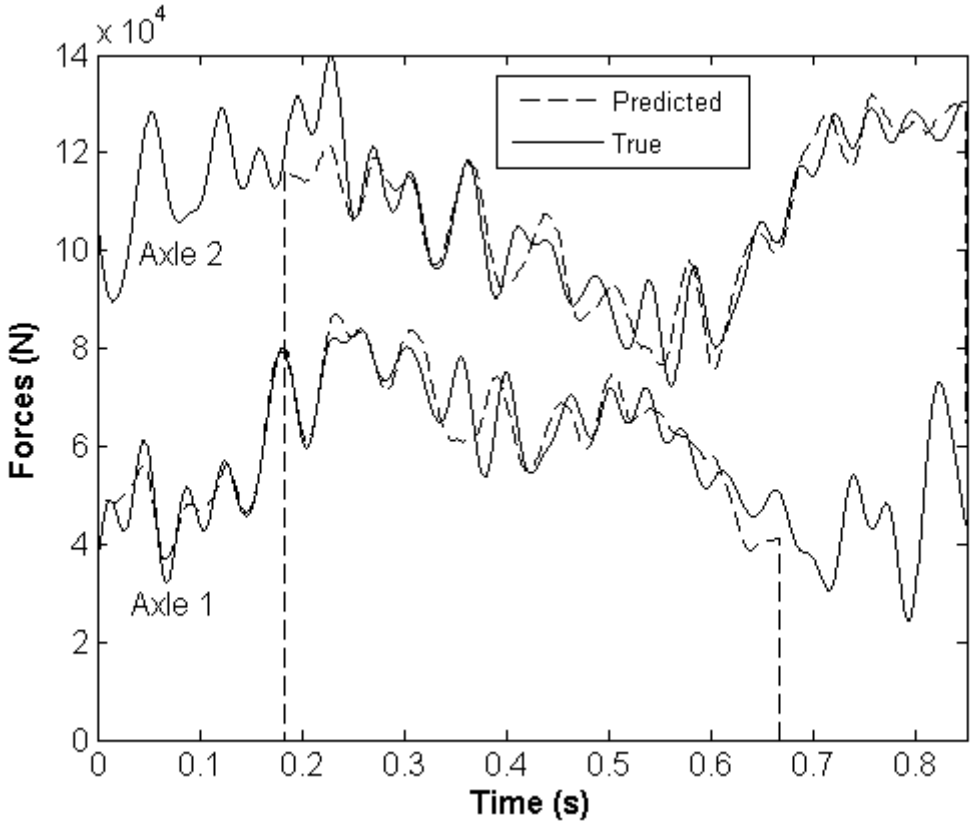
x 10^4
14
12
10
8
6
4
2
0
Forces (N)
Predicted
True
Axle 2
Axle 1
0
0.1
0.2
0.3
0.4
0.5
0.6
0.7
0.8
Time (s)

Figure 6

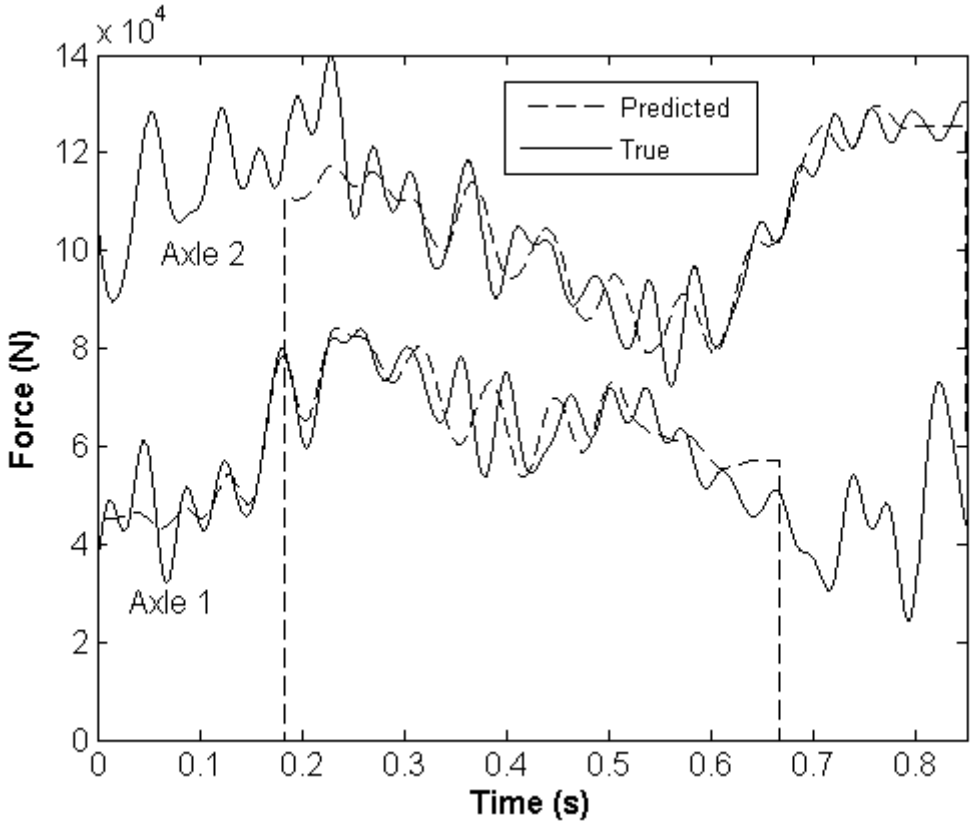
x 10^4
14
12
10
8
6
4
2
0
Force (N)
Predicted
True
Axle 2
Axle 1
0
0.1
0.2
0.3
0.4
0.5
0.6
0.7
0.8
Time (s)

Figure 7

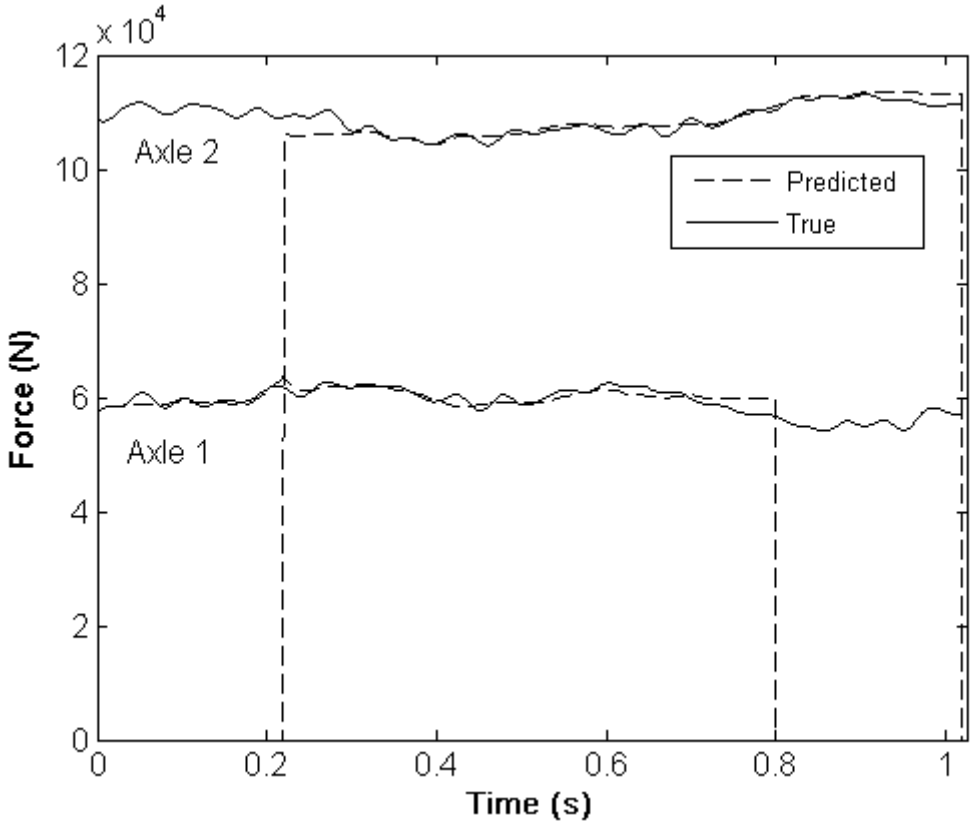
x 10^4
12
10
8
6
4
2
0
Force (N)
Axle 2
Axle 1
Predicted
True
0
0.2
0.4
0.6
0.8
1
Time (s)

Figure 8

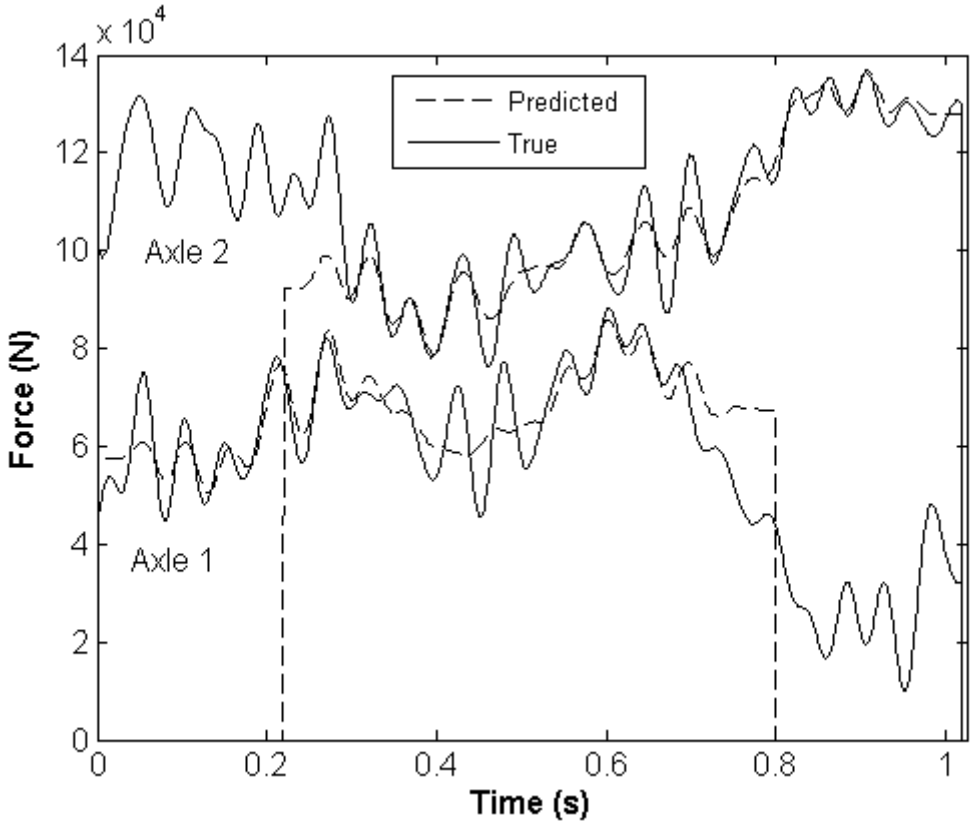
x 10^4
14
12
10
8
6
4
2
0
Force (N)
Predicted
True
Axle 2
Axle 1
0
0.2
0.4
0.6
0.8
1
Time (s)

Figure 9

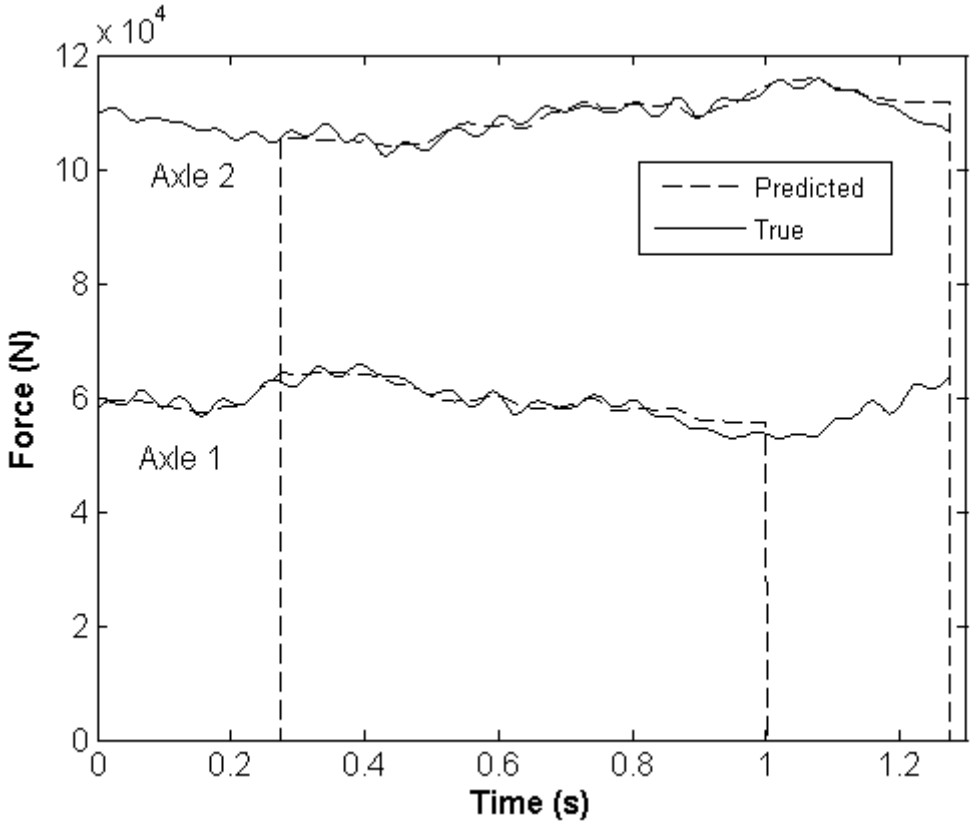
x 10^4
12
10
8
6
4
2
0
Force (N)
Axle 2
Axle 1
Predicted
True
0
0.2
0.4
0.6
0.8
1
1.2
Time (s)

Figure 10

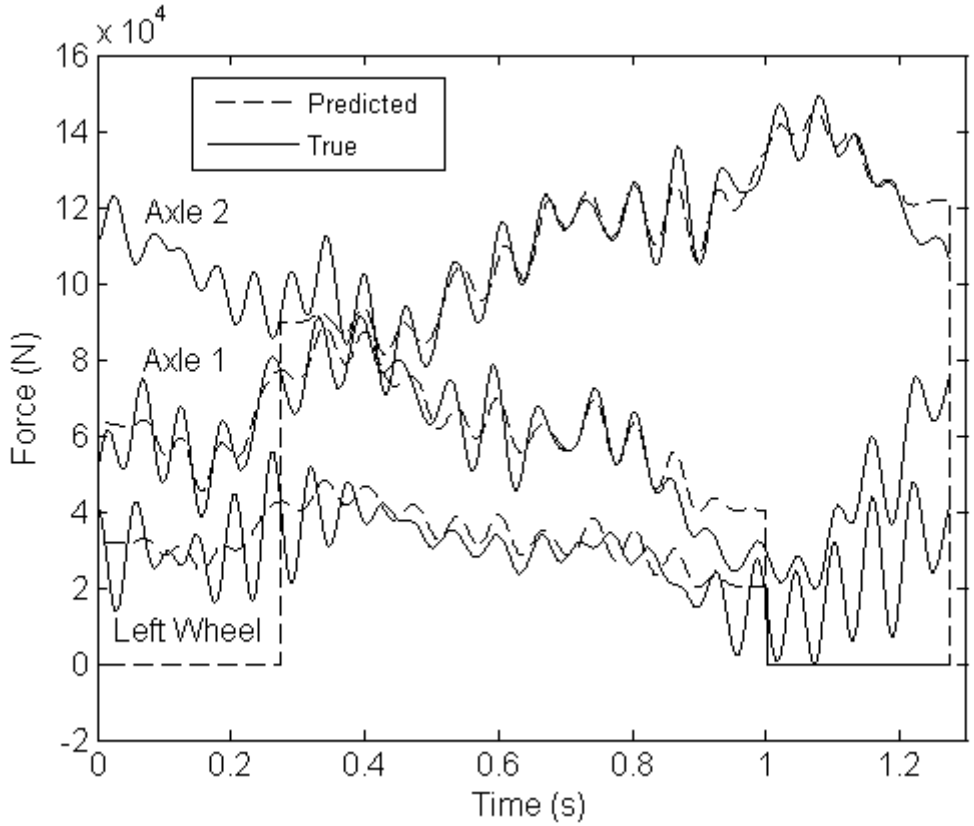
x 10^4
16
14
12
10
8
6
4
2
0
-2
Force (N)
Predicted
True
Axle 2
Axle 1
Left Wheel
0
0.2
0.4
0.6
0.8
1
1.2
Time (s)

Figure 11

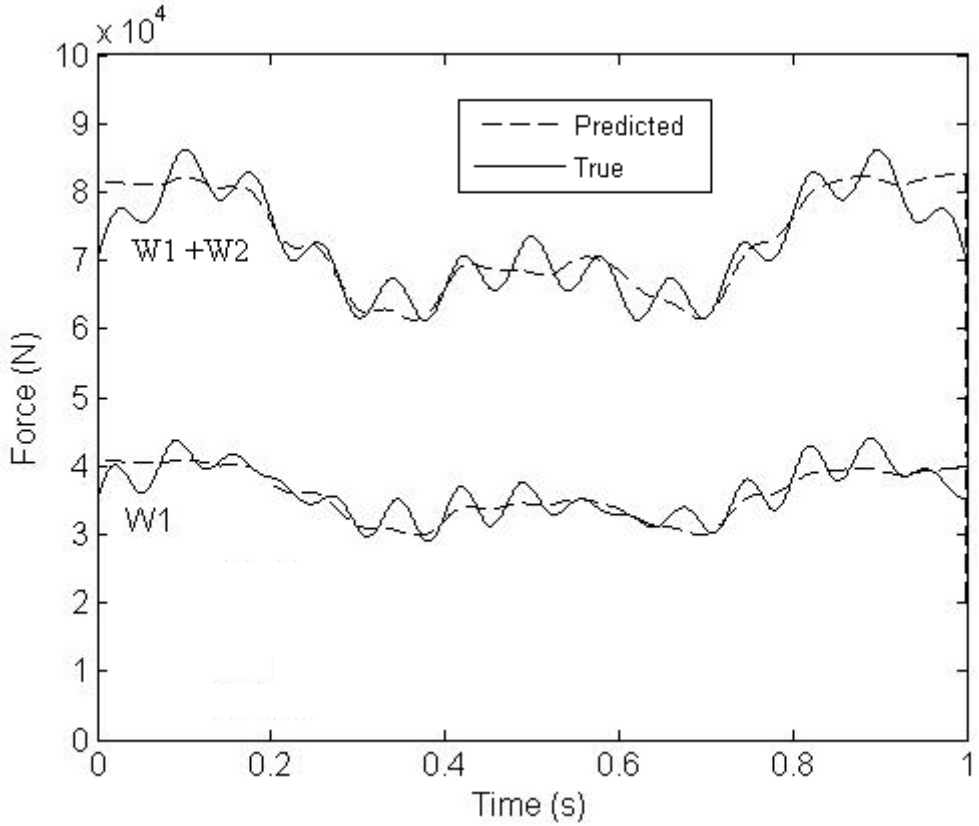
x 10^4
10
9
8
7
6
5
4
3
2
1
0
Force (N)
Predicted
True
W1 +W2
W1
0
0.2
0.4
0.6
0.8
1
Time (s)

Figure 12

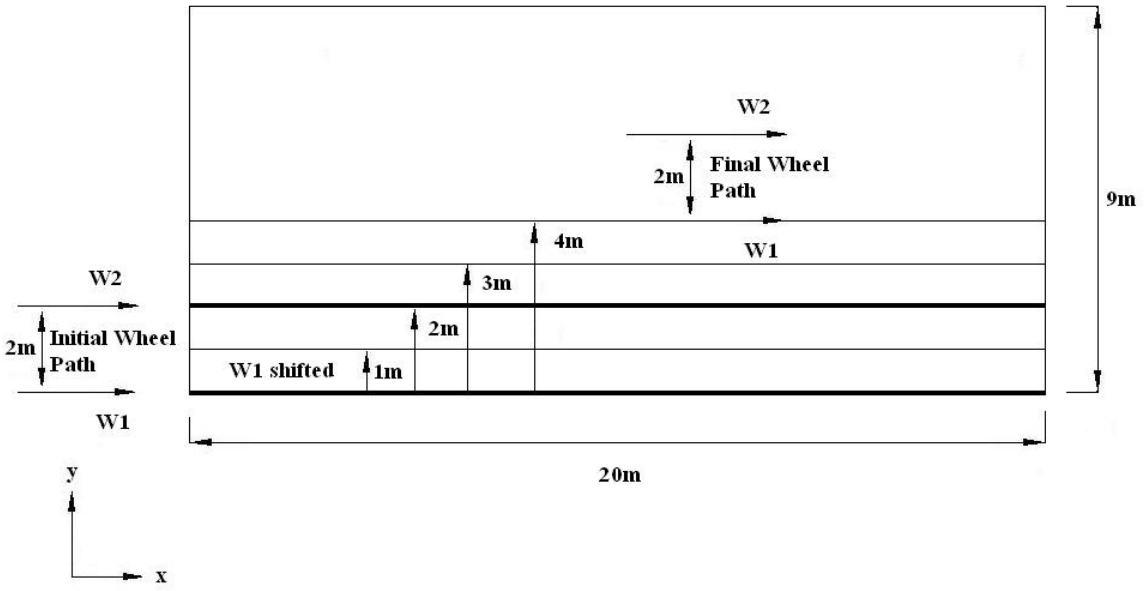
W2
2m
Final Wheel
Path
9m
4m
W1
W2
3m
2m
2m
Initial Wheel
Path
W1 shifted
1m
W1
20m
y
x

Figure 13